



# Skeleton growing and pruning with bending potential ratio

Wei Shen<sup>a</sup>, Xiang Bai<sup>a,\*</sup>, Rong Hu<sup>a</sup>, Hongyuan Wang<sup>a</sup>, Longin Jan Latecki<sup>b</sup>

<sup>a</sup> Huazhong University of Science and Technology, Wuhan, China

<sup>b</sup> Temple University, Philadelphia, USA

## ARTICLE INFO

### Article history:

Received 23 August 2009

Received in revised form

31 July 2010

Accepted 14 August 2010

### Keywords:

Skeleton

Skeleton pruning

Skeleton growing

Bending potential ratio

## ABSTRACT

We propose a novel significance measure for skeleton pruning, called bending potential ratio (BPR), in which the decision regarding whether a skeletal branch should be pruned or not is based on the context of the boundary segment that corresponds to the branch. By considering this contextual information, we can better evaluate the contribution of the boundary segment to the overall shape, which generally depends on its particular location within the whole contour (i.e., a segment may be considered to be insignificant in one place while it may be considered as a feature elsewhere). The BPR is a measure of the significance of contour segments in such context, and depicts the bending potential of a contour segment. Unlike other significance measures that only contain local shape information, the BPR evaluates both local and global shape information. Thus, it is insensitive to local boundary deformation. In addition, we also present a scheme for skeleton growing, which integrates pruning based on the BPR measurement. Our experiments demonstrate that the skeletons obtained by the proposed algorithm are medially placed and connected. We also demonstrate that shapes reconstructed from these skeletons are very close to the original shapes. Moreover, the BPR measure yields a natural multi-scale skeletal representation.

© 2010 Elsevier Ltd. All rights reserved.

## 1. Introduction

Skeleton is a very useful shape descriptor, since it contains shape features of the original object. Thus, skeleton is essential for shape representation and analysis in many application areas such as content-based image retrieval systems, character recognition systems, circuit board inspection systems, and analysis of biomedical images [2]. Skeleton, which is also called *medial axis*, was first defined by Blum [1] with a grassfire model.

In the past decades, various skeleton extraction methods have been proposed. Generally, they can be coarsely classified into five types: the thinning algorithms [3,4,29], the discrete domain algorithms based on the Voronoi diagrams [5,6,8], the algorithms based on distance transform [7,11,12,30,31,32,33], iterative shrinking of the object contour [14,16,22], and the algorithms based on mathematical morphology [9]. Those methods have a common drawback, which is their high sensitivity to the boundary noise: small errors in the object boundary can drastically change the derived skeleton [10]. Consequently these methods may often yield spurious skeleton branches, which negatively influences the performance of object recognition based

on skeletal structure. Hence, it is necessary to prune the spurious skeleton branches.

Many approaches have been developed for skeleton pruning. Some of them smooth the boundary before the computation of skeletal points, which aim to remove unwanted boundary noise and discretization artifacts [36,39,46]. However, boundary smoothing may change the boundary location, and consequently, the skeleton position may shift, which is due to the difficulty in distinguishing noise from low frequency shape information on boundaries [20]. Others try to assign a significance measure to each skeleton point or skeleton branch, and then the skeleton points/branches are pruned when their significance values are less than a given threshold. A few important methods based on significance measure need to be mentioned: Ogniewicz and Kübler [15] presented several length based significance measures for a given skeleton point, such as the length of the chord between two *generating points* (the points of the maximal disk centered at the skeleton point, which are tangent to the boundary) and the length of the shortest boundary segment between two generating points. Shaked and Bruckstein [13] summarized such methods, and they suggest choosing the maximal erosion thickness as the significance measure. Couprie and Zour [17] proposed another significance measure named bisector angle, which is the angle between the lines connecting the skeleton point and its generating points. These significance measures suffer from similar drawbacks. First, some redundant skeleton branches may not be removed completely, which constrains the shape matching based

\* Corresponding author.

E-mail addresses: shenwei1231@gmail.com (W. Shen), xiang.bai@gmail.com (X. Bai), hr@smail.hust.edu.cn (R. Hu), wythywl@public.wh.hb.cn (H. Wang), latecki@temple.edu (L. Jan Latecki).

on skeletal structure as illustrated in Fig. 1b. Second, the pruning results are not multi-scale. The concept of multi-scale skeleton is outlined in [23], which appeals well to human intuition in that on a coarse scale the skeleton represents the significant visual parts of the shape, whereas, on a fine scale, the skeleton contains more small details such as the tip of the trunk in Fig. 1. Third, sometimes the pruning results are inconsistent with our intuition as illustrated in Fig. 2. In Fig. 2a and b,  $q_1$  and  $q_2$  are the generating points of  $p$ ; observe that the contour segment between  $q_1$  and  $q_2$ , the forelimb of the mouse, gives rise to no skeleton branches since both the length of chord  $\overline{q_1q_2}$  and the angle  $\angle q_1pq_2$  are small. Obviously, the pruning results are inconsistent with human perception, because the forelimb is a significant part of the whole body and should generate skeleton branches as shown in Fig. 2c.

Recently, Ward and Hamarneh [18] gave an unconventional pruning method named groupwise pruning, assuming that shapes in the same class have common shape information encoded into their skeletons. They utilize the similarity of the skeletons of the objects in the same class to determine the significance of skeleton branches by group information. Although their method exhibits excellent pruning outcomes, the assumption of this method may not be general for many cases, because the shapes from the same class can differ significantly due to in-class variation, distortion or non-rigid transformation [19]. In addition, the computational complexity of this method is much higher than any other methods. Bai et al. [20] proposed an effective and elegant pruning method, which can be integrated into a skeleton extracting process. The main idea is partitioning the object's contour into segments by discrete curve evolution (DCE) [21], followed by eliminating the skeleton points whose generating points are on the same segment. The method of Bai et al. compares very favorably to all of the above methods, and the pruned skeletons have been successfully applied to skeleton graph matching [27] and object recognition in natural images [45]. However, the obtained skeletons may contain some redundant points and some unimportant branches as shown in Fig. 3.

To summarize, all existing methods are deficient in some respect. The major drawback of the pruned skeletons is that they may contain many spurious skeleton branches. For the example in Fig. 1, we view the hand-labeled skeleton in (d) as the reference skeleton. Any skeleton branch that is not included in the skeleton (d) is regarded as a spurious branch. The skeleton in (a) has about 400 spurious branches, the one in (b) 87 spurious branches, and the one in (c) only one spurious branch (located in the tip of the trunk).

This paper deals with the problems mentioned above. It presents a novel significance measure, called *bending potential ratio* (BPR), which can be used to remove spurious skeleton branches. According to Blum's definition of skeleton [1], a skeleton is generated from the boundary and each skeleton branch corresponds to a contour segment. Our intuition is that only contour segments that are significant in the context of the whole contour should give rise to skeleton branches. Conversely, the skeleton branches originating from insignificant contour segments are spurious and should be pruned. It is difficult to make correct decision based only on the shape's outline regarding whether a skeletal segment is significant or not. Therefore, we propose that the context also includes the location of the segment in the whole contour, since the contribution of the same segment to the overall shape may be different when the location is different in the whole contour. A segment may be considered to be insignificant in one place while it may be considered as a feature in another place, as shown in Fig. 6. BPR is a measure of the significance of contour segments in such context, which depicts the bending potential of a contour segment. Unlike other significance measures that only contain local shape information, BPR integrates both local and global shape information. Thus, it is insensitive to local boundary deformation. Moreover, the pruning results based on BPR are multi-scale and can represent visual parts of the object. In addition, we also present a scheme for skeleton growing, which integrates pruning based on BPR measurement. During skeleton growing, spurious skeleton

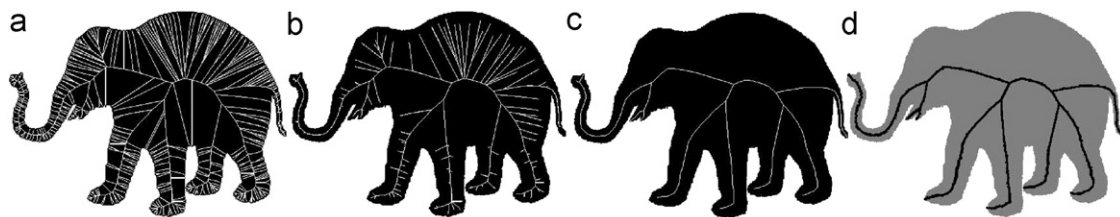


Fig. 1. (a) The skeleton of an elephant obtained by the method in [12]; (b) the pruning result of (a) using the significance measure of the length of the chord [15]; (c) the skeleton generated by the proposed method; (d) the hand-labeled skeleton.

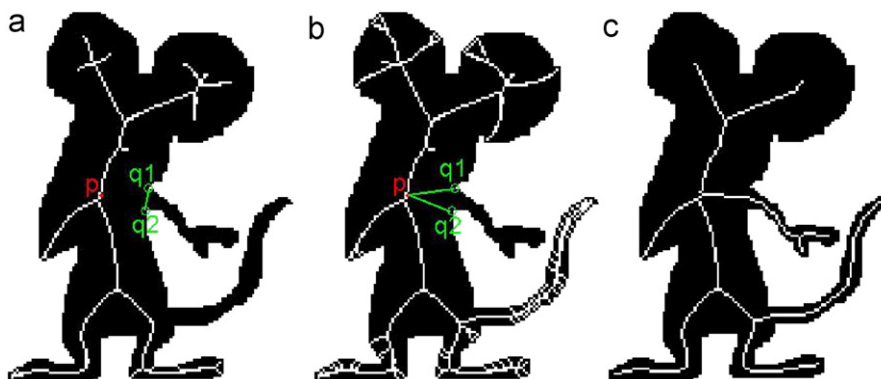
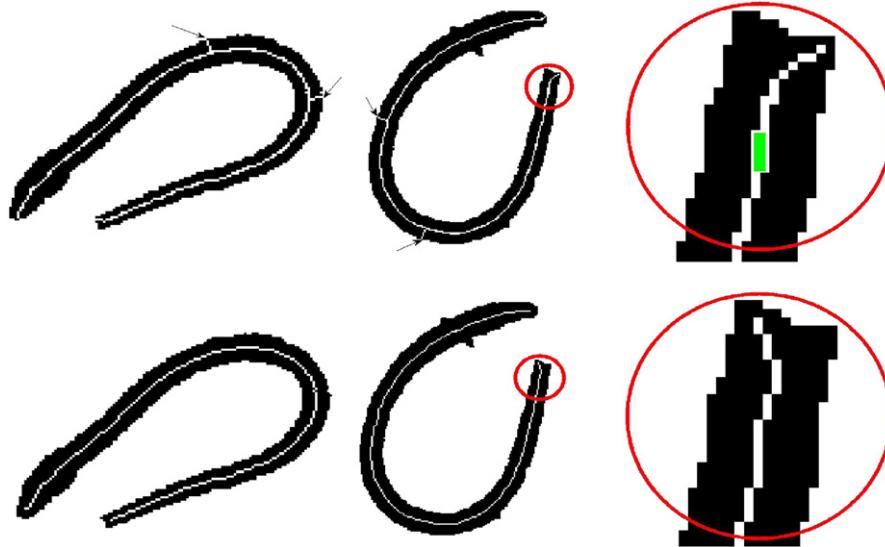


Fig. 2. (a) A pruned skeleton obtained based on the significance measure of the length of the chord [15]. (b) A pruned skeleton obtained based on the significance measure of the bisector angle [17]. (c) The skeleton pruned by the proposed significance measure.



**Fig. 3.** First row: The skeletons of two sea snake shapes obtained by the method in [20]. The boundary points pointed to by arrows generate unimportant skeleton branches and some parts of the skeletons contain redundant points, such as the green points in the red circle area (showed zoomed). Second row: The skeletons of the same shapes obtained by the proposed method.

branches are eliminated and the connectivity of the obtained skeleton is guaranteed by the skeleton growing process.

The rest of this paper is organized as follows. In Section 2, we recall some basic notation for binary images. In Section 3, we define the BPR significance measure. In Section 4, a scheme for skeleton growing based on BPR is presented. Experimental results and analysis are presented in Section 5. Finally, the conclusions are given in Section 6.

## 2. Basic notation

For simplicity of presentation, we assume that the boundary contour of a 2D object is a simple closed curve  $C$  in  $R^2$ . The bounded set  $F$  inside contour  $C$  represents the region of the object. All our definitions and statements apply also to a planar set  $F$  whose boundary contour is composed of a finite number of simple closed curves, i.e.,  $F$  may have a finite number of holes, since if a skeleton point originated from two different contour curves it will never be removed from the skeleton. Therefore, any skeleton point that is removed originates from a single contour curve, and consequently, we focus on the case of a single contour curve  $C$ .

Given a point  $p$ , which we state in the image domain, where the term point refers to a pixel, we define the function of distance transform  $\kappa$  as

$$\kappa(p) = \begin{cases} \min_{v \in C} d(p, v), & p \in F, \\ 0, & p \notin F, \end{cases} \quad (1)$$

where  $d(\cdot, \cdot)$  is the Euclidean distance measure.

For a point  $p \in F$ ,  $r(p)$  denotes a set of nearest contour points to  $p$ . Obviously,

$$d(p, r(p)) = \kappa(p). \quad (2)$$

With  $r(p)$  we have the following definition of *ruling points*  $R(p)$ :

**Definition 1.** We define *ruling points*  $R(p)$  as a set of points on the contour  $C$  that are the closest to a point  $p$  or its eight-neighborhood inside the contour, i.e.,

$$R(p) = R_8(p) \cup r(p) = \{r(q) | q \in N_8(p)\} \cup r(p), \quad (3)$$

where  $N_8(p)$  are the eight neighbors of point  $p$  inside the contour and  $R_8(p) = \{r(q) | q \in N_8(p)\}$ .

Obviously, if  $p$  is a skeleton point,

$$n(R(p)) \geq 2, \quad (4)$$

where function  $n(\cdot)$  denotes the number of the elements in a set.

In accord with our statement at the beginning of this section, the concept of a ruling point easily extends to a set  $F$  whose boundary is a union of simple closed curves  $C_1, \dots, C_k$ . Then a point  $p$  is a ruling point if it is a ruling point with respect to any  $C$  in  $\{C_1, \dots, C_k\}$ . All other concepts and properties presented in this paper extend in the same way.

## 3. Bending potential ratio

### 3.1. Definition of bending potential ratio

Consider two points  $q_1, q_2 \in R(p)$  ( $n(R(p)) \geq 2$ ) shown in Fig. 4, the shortest contour segment between  $q_1$  and  $q_2$  is denoted as  $C(q_1, q_2)$ . Since the contour segment is a digital set consisting of pixels, we measure the length of the contour segment by the total distance between each pair of neighboring pixels, and according to the Euclidean metric, the distance between two neighboring pixels displaced horizontally/vertically is 1 and diagonally is  $\sqrt{2}$ . If  $q_1$  and  $q_2$  divide the contour into two segments of equal length, arbitrarily one of them is denoted as  $C(q_1, q_2)$ .

**Definition 2.** For a contour segment  $C(q_1, q_2)$ , let  $l(q_1, q_2)$  denote the arc length of  $C(q_1, q_2)$ . We construct an isosceles triangle with base  $q_1 q_2$  and with a vertex  $g \in R^2$  such that

$$d(g, q_1) = d(g, q_2) = \frac{1}{2}l(q_1, q_2). \quad (5)$$

There are actually two different points satisfying formula (5), which are marked with  $g_1$  and  $g_2$  in an example shown in Fig. 5c, and the arbitrary one can be chosen as the point  $g$ , e.g.,  $g_1$  in Fig. 5c. We call the so defined point  $g$  a ghost point of  $C(q_1, q_2)$ .

Usually, the ghost point  $g$  does not lie on the contour, unless the contour segment is a symmetrical polygonal line as shown in Fig. 5b. If  $g$  lies on the contour as shown in Fig. 5a, then obviously,  $l(g, q_1) > d(g, q_1)$ ,  $l(g, q_2) > d(g, q_2)$ ,  $l(q_1, q_2) > d(g, q_1) + d(g, q_2)$ , and  $g$  would not satisfy formula (5).

**Definition 3.** Let point  $p$  lie inside the contour  $C$  with  $n(R(p)) \geq 2$ , and let  $q_1, q_2$  be two points in  $R(p)$ . Let point  $g$  be the ghost point of the contour segment  $C(q_1, q_2)$ . With reference to Fig. 4, let  $h_g$  be the height of triangle  $q_1q_2g$  and let  $h_p$  be the height of triangle  $q_1pq_2$ . The bending potential ratio (BPR)  $\varepsilon(p, q_1, q_2)$  is defined as

$$\varepsilon(p, q_1, q_2) = \frac{h_g}{h_p}. \tag{6}$$

### 3.2. Discussion of bending potential ratio

As shown in Fig. 4, since  $\Delta q_1q_2g$  is an isosceles triangle, it is not difficult to obtain that

$$h_g = \frac{1}{2} \sqrt{l^2(q_1, q_2) - d^2(q_1, q_2)}. \tag{7}$$

Observe that  $h_g$  provides local information of the contour segment  $C(q_1, q_2)$ , since the arc length  $l(q_1, q_2)$  and the chord length  $d(q_1, q_2)$  are its own properties. For a fixed distance  $d(q_1, q_2)$ , the larger the  $l(q_1, q_2)$  is, the more bendable the  $C(q_1, q_2)$  is. Hence,  $h_g$  reflects the bending potential of the contour segment  $C(q_1, q_2)$ . A contour segment with a sharp bend contains a point with locally maximal curvature, and there is a connection between the positive curvature maxima of the shape boundary and the skeleton in the sense that each curvature maximum gives rise to a skeletal branch [24]. Consequently,  $h_g$  can be considered as a measurement for estimating the significance of a contour segment.

By trigonometry, we have

$$\frac{1}{2} h_p d(q_1, q_2) = \frac{1}{2} d(p, q_1) d(p, q_2) \sin(\angle q_1 p q_2) \tag{8}$$

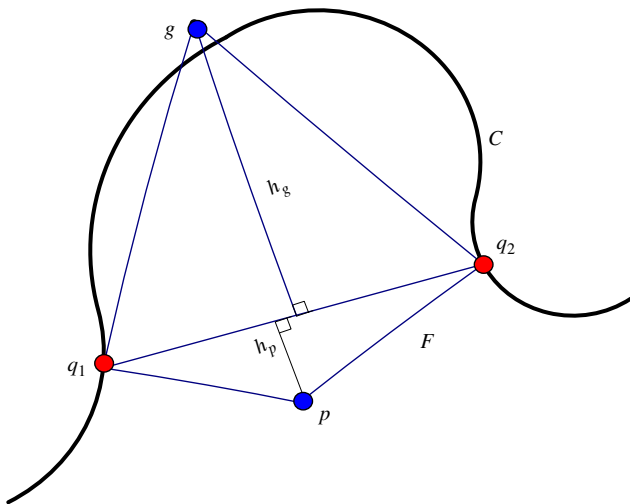


Fig. 4. The definition of ghost point and BPR.

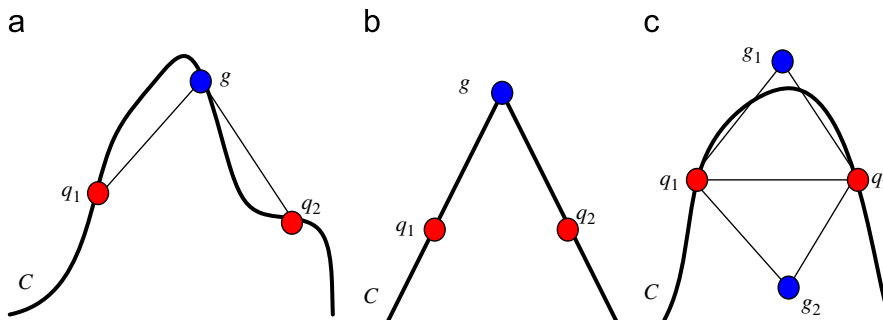


Fig. 5. The location of ghost point.

and we have

$$h_p = \frac{d(p, q_1) d(p, q_2) \sin(\angle q_1 p q_2)}{d(q_1, q_2)}. \tag{9}$$

If  $p$  is a skeleton point,  $d(p, q_1)$  is approximately equal to  $d(p, q_2)$ ; hence we obtain

$$h_p = d(p, q_1) \cos\left(\frac{\angle q_1 p q_2}{2}\right). \tag{10}$$

Formula (10) expresses that  $h_p$  contains not only the information of the bisector angle [17] but also the width of the object. Whether a contour segment is significant or not is determined by not only its own information, e.g. the arc length, but also the context where it is located. The same contour segment may more likely be considered to be insignificant if it locates on a broad part of shape, while if it locates on a narrow part of shape, it may be prone to be considered as a feature. Hence, the ratio of  $h_g$  and  $h_p$ , the bending potential ratio integrates both local and global shape information. It can be used to determine whether a contour segment generates a skeleton branch. Particularly,  $h_p$  is 0 if the tangents in  $q_1$  and  $q_2$  are parallel. In this case, the BPR value is infinite, which indicates that  $p$  is a skeleton point. Fig. 6 contains an illustrative example showing the effect of BPR in pruning skeletons. The peaks in Fig. 6 are the same; however, they have different shape contributions to the objects. The peak in Fig. 6a is more likely to be a negligible detail on the boundary, and so the branch originating from it should be pruned, while the peak with the same size in Fig. 6b is more likely to be an important shape feature, and so it should generate a skeleton branch. The peak in Fig. 6c is closer to the right angle than the peak in Fig. 6a, and consequently, it gives rise to a skeleton branch, since it replaces the right angle as the feature of the shape. As shown in Fig. 6, the skeletons obtained by our method can distinguish between a negligible branch as in (a) and significant branches as in (b, c). In the differential geometry, the bending of a planar curve at a given point is measured by its curvature, where the curvature is a strictly local property and measures the behavior of the curve at a given point. In contrast, the proposed BPR is a global property; in particular, it depends on the placement of a contour segment within the whole contour as demonstrated in Fig. 6.

### 3.3. Relation of BPR to other significance measures

We note a formal connection between BPR and other significance measures, such as the length of chord [15], the length of shortest boundary segment [15], and the bisector angle [17]. Linking our significance measure to others is helpful to understand the advantage of BPR.

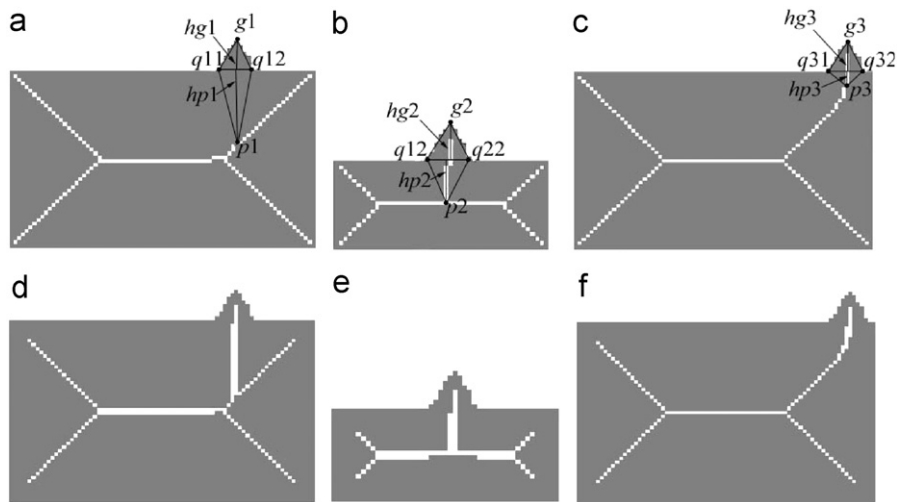


**Fig. 6.** Samples of rectangles with the same peak added to their boundary. First row: The skeletons obtained by proposed method. Second row: The skeletons of the same shapes pruned by the significance measure of the length of the shortest boundary segment proposed in [15].  $p_i$  ( $i=1, 2, 3$  in (a), (b), (c), respectively) is the point under consideration,  $q_{i1}, q_{i2} \in R(p_i)$ , and the  $g_i$  is the ghost point. The peaks all give rise to skeleton branches based on the significance measure in [15] (set  $l(q_{i1}, q_{i2}) \geq 10$ ), since they are the same. Based on our significance measure (set  $h_{g_i}/h_{p_i} \geq 0.8$ ), the pruning results are different.

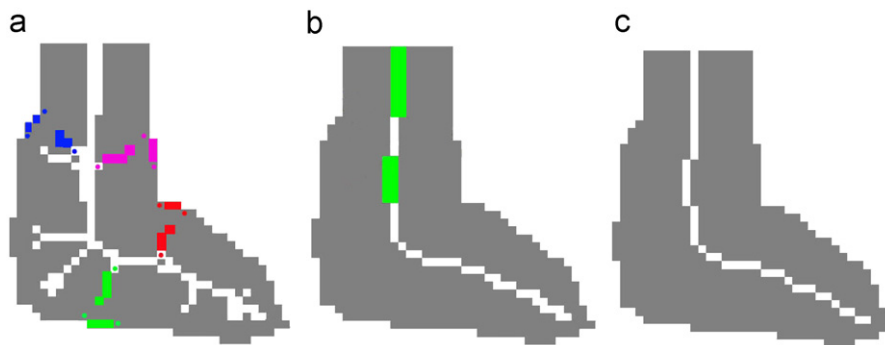


**Fig. 7.** The skeletons of a camel foot. The skeleton in (a) was generated by the approach in [12]. The boundary points marked with color dots are the ruling points of skeleton points marked with dots of the same color. (b) The skeleton generated by Criterion 1 contains some redundant points, as the green part. (c) The skeleton obtained by applying the method in [3] to the skeleton in (b).

By formulae (6), (7), and (10), we obtain

$$\varepsilon(p, q_1, q_2) = \frac{h_g}{h_p} = \frac{(1/2)\sqrt{P(q_1, q_2) - d^2(q_1, q_2)}}{d(q_1, q_2)/2 \tan(\angle q_1 p q_2 / 2)} = \tan\left(\frac{\angle q_1 p q_2}{2}\right) \sqrt{\frac{P(q_1, q_2)}{d^2(q_1, q_2)}} - 1. \quad (11)$$

Formula (11) expresses the connection between BPR and the significance measures: the length of the chord  $d(q_1, q_2)$ , the length of the shortest boundary segment  $l(q_1, q_2)$ , and the bisector angle  $\angle q_1 p q_2$ . A proper integration of the three measures is one of the main contributions of the proposed method. It is reasonable to integrate the other three measures in this way, since the larger the  $\angle q_1 p q_2$  is, the more possible  $p$  is a skeleton point, and the tangent function reinforces this trend, particularly when  $\angle q_1 p q_2 = \pi$  (the maximum value), the BPR value is infinite. Moreover, the ratio of the other two  $l(q_1, q_2)/d(q_1, q_2)$  has the property that the local maxima of it often correspond to limb-like parts [28], and limb-like parts always give rise to skeleton branches. Therefore, it is more accurate to use the product of these measures to determine whether a contour segment should generate a skeleton branch. Using any one of the other three measures may lead to incorrect results as shown in Fig. 2b. While  $\angle q_1 p q_2$  is small, since  $l(q_1, q_2)/d(q_1, q_2)$  corresponds to a long forelimb in Fig. 2, the value of  $l(q_1, q_2)/d(q_1, q_2)$  is pretty large. Therefore, the value of BPR is still large enough to indicate that the contour segment  $C(q_1, q_2)$  should generate skeleton.

#### 4. A scheme for pruned skeleton growing

Now, we propose a scheme for skeleton growing recursively by adding points that satisfy a criterion based on BPR.

##### 4.1. The criterion for pruning the spurious branches

A criterion introduced in [12], which is based on the ruling points, is used to determine whether the given point is a skeleton point. It is the reason why we call them ruling points. We briefly review the criterion here in the image domain: For a given point  $p$  inside contour  $C$  with  $n(R(p)) \geq 2$ , if there exists  $q_1 \in r(p)$  and  $q_2 \in R_8(p)$  that satisfies

$$d^2(p, q_1) - d^2(p, q_2) \leq \max(\text{abs}(x_1 - x_2), \text{abs}(y_1 - y_2)), \quad (12)$$

the point  $p$  is considered to be a skeleton point, where  $(x_1, y_1)$  and  $(x_2, y_2)$  are the coordinates of  $q_1$  and  $q_2$ , respectively. Based on formula (12), the skeleton is medially placed in the silhouette region and connected [12], but the skeleton contains too many spurious skeleton branches, e.g., the colored branches shown in Fig. 7a. Note that the spurious skeleton branches marked with color are generated from insignificant contour segments of the same color. The proposed significance measure BRP solves this

problem. We modify the criterion in [12] as follows:

**Criterion 1.** Point  $p$  belongs to the pruned skeleton if there exist  $q_1 \in r(p)$  and  $q_2 \in R_8(p)$  that satisfy

$$\begin{cases} d^2(p, q_1) - d^2(p, q_2) \leq \max(\text{abs}(x_1 - x_2), \text{abs}(y_1 - y_2)), \\ \varepsilon(p, q_1, q_2) > t, \end{cases} \quad (13)$$

where  $t$  is a given threshold, and  $(x_1, y_1)$  and  $(x_2, y_2)$  are the coordinates of  $q_1$  and  $q_2$ , respectively.

Obviously, Criterion 1 is a necessary condition to determine whether a shape point is a skeletal point, and based on the proposed significance measure, just the pairs of contour points connecting significant contour segments are used to determine whether the corresponding points are skeleton points. Hence, the spurious skeleton branches are not produced by the modified criterion.

#### 4.2. Growing a pruned skeleton

Based on the above criterion, we give the scheme for growing a pruned connected skeleton. For a 2D object, the bounded set  $F$

inside contour  $C$  represents the region of the object, and  $Sk$  is the skeleton of the object.

**Procedure SkeletonGrow (Input  $F$ , Output  $Sk$ )**

01. Choose the point  $p_m \in F$ , such that  $\kappa(p_m)$  is maximum.
02. **If**  $p_m$  satisfies Criterion 1
03.     add  $(p_m, \kappa(p_m))$  to  $Sk$  and push  $p_m$  to a stack  $S$
04. **End**
05. **While**  $S$  not empty
06.      $p \leftarrow \text{pop}(S)$
07.     **For** 8 neighbors  $x$  of  $p$  that satisfy Criterion 1
08.         Add  $(x, \kappa(x))$  to  $Sk$ , push  $x$  to  $S$
09.     **End**
10. **End**

The skeleton based on the proposed scheme is shown in Fig. 7b, the spurious skeleton branches have been pruned. Some part of the obtained skeleton may contain redundant points, like the green part shown in Fig. 7b. In many shape matching methods based on skeletal structure, sampling some points from skeletons or detecting critical points (end points and junction points) is

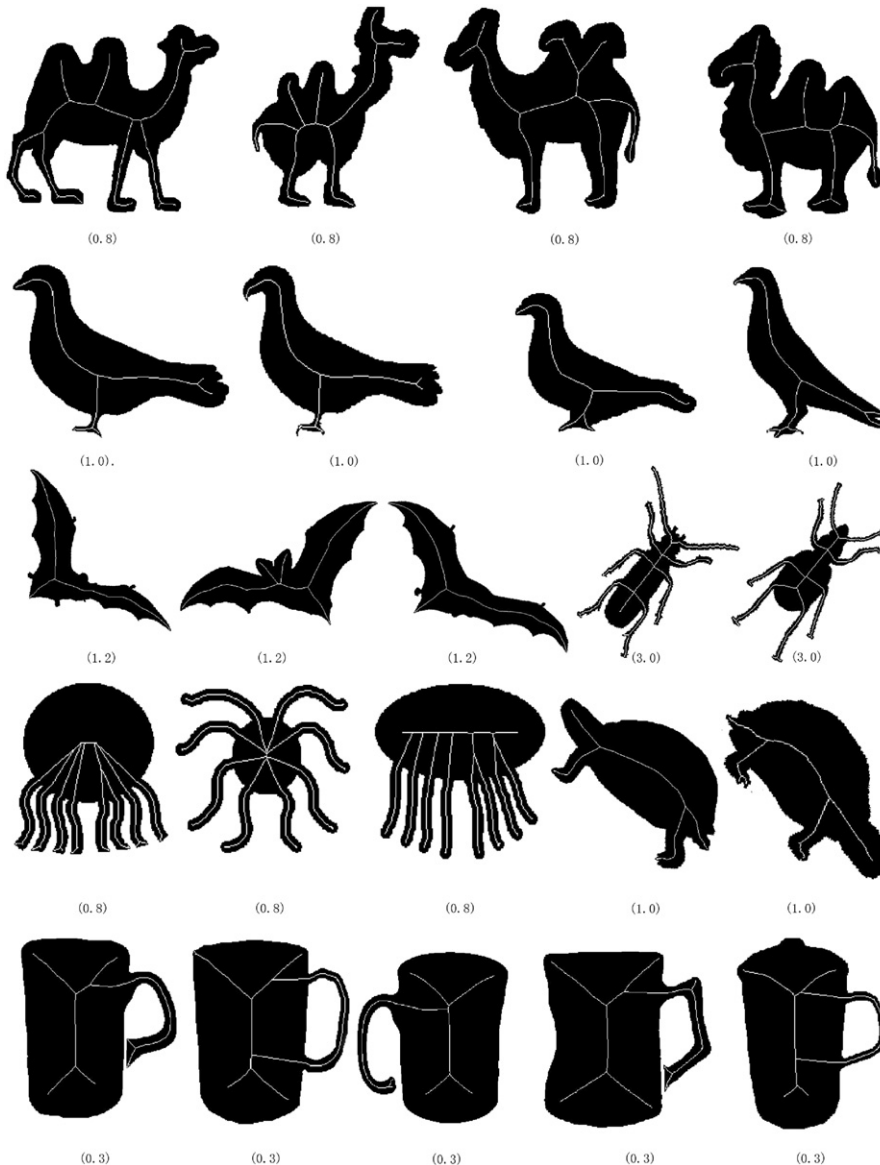


Fig. 8. Selected pruning results on MPEG-7 shape data set; the threshold values  $t$  set in experiment are shown in brackets.

needed, such as the method in [27,43,44]. Removing the redundant points from skeletons will benefit shape matching and analysis. To achieve this, any topology preserving removal operations [32] can be applied to the pruned skeleton. We used a morphological thinning method proposed in [3] and the result is shown in Fig. 7c.

#### 4.3. Computational complexity

The time complexity of our approach is described in this section. In order to calculate BPR, we need to parameterize the boundary by the arc length, which has complexity  $O(m)$ , where  $m$  is the number of boundary points. For a point  $p$  to be checked whether it should be added to the skeleton, the number of its ruling points is  $n$ . Checking whether point  $p$  satisfies Criterion 1 has complexity  $O(n)$  [12]. Thus, the total time complexity of our approach is  $O(nN+m)$ , where  $N$  is the number of pixels inside the boundary. Actually, in real application,  $n$  is often equal to a smaller value, like 3 or 4, and  $m$  is much less than  $N$ ; thus our algorithm is fast. On a 1.61 GHz AMD Sempron computer, it takes about 7 s in average to extract the pruned skeleton from a  $512 \times 512$  image.

## 5. Experimental results

First, we show the stability of the proposed approach in relation to shape deformations and boundary noise. Then, we

present comparison to state-of-the-art approaches. Next, the discussion about the effect of the threshold value  $t$  is given. After that, we evaluate the quality of pruned skeletons. Finally, we demonstrate that the obtained skeleton can be useful in shape matching.

#### 5.1. Stability

Some selected results on shapes from MPEG-7 Core Experiment CE-Shape-1 data set [26] are shown in Figs. 8 and 9. There are 70 groups of objects in MPEG-7 data set, some of them having complex shapes and boundary noise insertions. Note that like the experiments in [35], for different shapes of the same class, we use the same threshold, which is very important for automatic recognition with skeletons. In Fig. 8, several objects from the same class are put together, although their shape differs significantly, the obtained pruned skeletons have similar structure, e.g., the skeletons of the camels.

The pruned skeletons of the objects whose shape is quite complex such as like beetles and octopuses still match the hand-labeled skeletons, which proves the robustness of the proposed approach. In the last row in Fig. 8, two of cup shapes contain a hole and the proposed approach is also applicable to these shapes.

In Fig. 9, the objects are presented as pairs, where the second one is obtained by the significant contour deformation and distortion of the first one. The skeletons extracted from the shapes noisy shapes are still clean and have similar geometrical structure to the skeletons extracted from the shapes of smooth

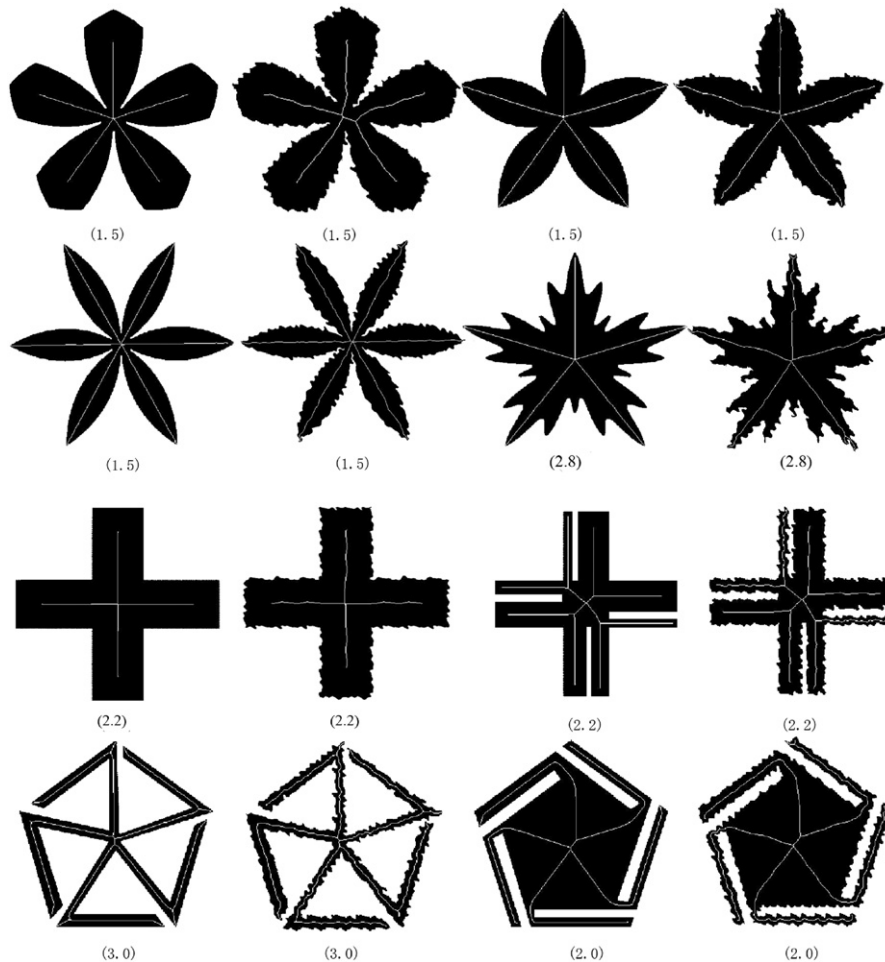
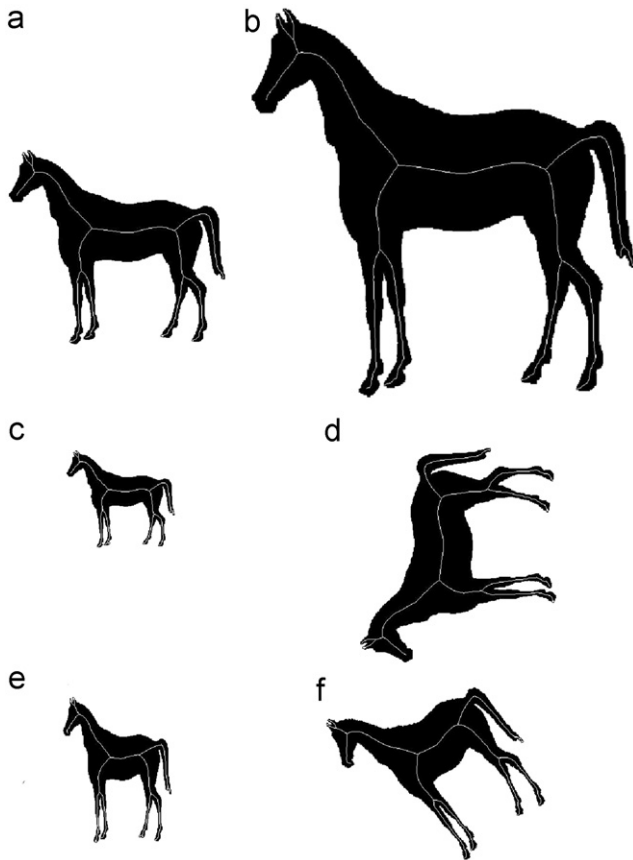


Fig. 9. Selected pruning results on MPEG-7 shape data set. The threshold values  $t$  set in experiment are shown in brackets.



**Fig. 10.** Skeletons generated by the proposed approach ( $t=1.0$ ) on shapes obtained by geometrical transformations: (a) original shape; (b) 2.0 scaling factor; (c) 0.5 scaling factor; (d)  $90^\circ$  rotation; (e) nonuniform scaling with 0.5 and 0.75 scaling factors on X and Y axes, respectively; (f) nonuniform scaling with 0.75 and 1.0 scaling factor on X and Y axes, respectively, and  $35^\circ$  rotation.

boundary, which indicates that the proposed approach is stable in the presence of boundary deformations.

Furthermore, the proposed approach is applied to shapes after geometrical transformations, like rotations and scaling, in Fig. 10. Observe that the obtained skeletons are stable.

## 5.2. Comparison to other approaches

Fig. 11 provides a comparison of our approach (the second column) to the method in [14] (the first column). The third column illustrates the skeletons obtained by the method in [12], which can be approximately considered as the medial axis defined by Blum [1]. The skeleton points obtained by our method correspond all to the centers of maximal inscribed discs, since they are a subset of the skeletons of the third column, whereas the method in [14] is a skeletonization algorithm based on a type of boundary propagation that does not enforce this property. Clearly, the skeletons in Fig. 11a and b are not positioned medially in the silhouette region, in particular, the parts of the second hump and the pull ring. In contrast, as shown in Fig. 11c and d, all of our skeleton points are exactly symmetrical to the shape boundary. In order to quantitatively demonstrate that our skeletons are more accurate than the skeletons in [14], we compute the error measure of skeletons proposed in [14]. We briefly describe the measure below. We apply our skeletonization approach to a simple shape (a rectangular region) with known skeleton (Fig. 12a). Then, we compare the skeletonization results for this shape for a variable amount of boundary noise (Fig. 12b–f). For

fairness, we test the same rectangles with the same noise as in [14]. The error measure of a noisy skeleton  $S$  to the zero-noise skeleton  $D$  is defined as

$$\text{Err}(S,D) = \frac{1}{N} \sum_{i=1}^N \sqrt{(S_x(i)-D_x(i))^2 + (S_y(i)-D_y(i))^2}, \quad (14)$$

where  $N$  is the number of skeleton points in  $S$ ,  $[S_x(i), S_y(i)]$  are the coordinates of the  $i$ th skeleton point in  $S$  and  $[D_x(i), D_y(i)]$  is the closest point in  $D$  to the point  $[S_x(i), S_y(i)]$ . The average error measure of the five types of noisy skeletons to the first one in Fig. 12 is shown in Table 1. This experimental result serves to illustrate that our skeletons are more accurate and more robust to noise than the approach by Krinidis and Chatzis [14] and approaches in [15,17,20].

We also compare our result with the pruning result by DCE [20]. A comparison is shown in Fig. 3, we give another comparison in Fig. 13. Since the skeletons obtained by the method in [20] are multi-scale, we give the results with a different number of vertices selected by DCE. The parameter  $N$  is the number of vertices in the simplified boundary polygon; thus,  $N \geq 3$ . Generally, it is adequate to assign a larger  $N$  to the shape with more vertices, such as “octopus”, and to assign a small  $N$  to the shape with fewer vertices, such as “apple”. The results by DCE are shown in the first and second columns in Fig. 13. Our results are shown in the third column. The skeletons in the first and second columns contain some unimportant branches, such as the one located on the rightmost tentacle of the octopus. The main part of the apple in Fig. 13 is similar to a ball, so the skeleton points should be positioned at the nearby region of the center of the ball as is the case for our result, but not be grown to the boundary as the results by the method in [20].

To compare the proposed significance measure, BPR, to the approaches proposed in [15,17], we extract several skeletons by the method proposed in [12] integrated with pruning based on these significance measures. Figs. 1 and 2 indicate that BPR is much more favorable than the significance measure of the length of the chord [15] and the significance measure of the bisector angle [17]. Fig. 14 depicts the comparison between the significance measure of the length of the shortest boundary segment [15] (the first three) and ours (the last one). Observe that, based on the significance measure of the length of the shortest boundary segment, when the threshold value is small, the extracted skeleton contains many spurious branches, when the threshold value increases, the spurious branches are shorter or disappear; however the vital skeleton branches that represent significant visual parts of objects, such as the leaves of the apple, disappear too. The result in Fig. 14d indicates that our significance measure is superior.

Our method is very adequate for extracting skeletons from circular shapes. If a shape is similar to a circle, the skeleton should be located at the center. This cannot be achieved by many other methods. We give a comparison to show the superiority of our method in Fig. 15.

## 5.3. The effect of the threshold $t$

The effect of different threshold values  $t$  on the skeletons of objects is illustrated in Fig. 16. As discussed in Section 1, the proposed significance measure, BPR, can be taken as a proper trade-off between different shape scales. Due to this, multi-scale skeletons can be obtained by setting different threshold values  $t$  for BPR. When the value of the threshold  $t$  increases, there are fewer branches in the skeleton, which represent significant visual parts of objects, and the trivial parts are ignored. This property is in accord with human visual perception.

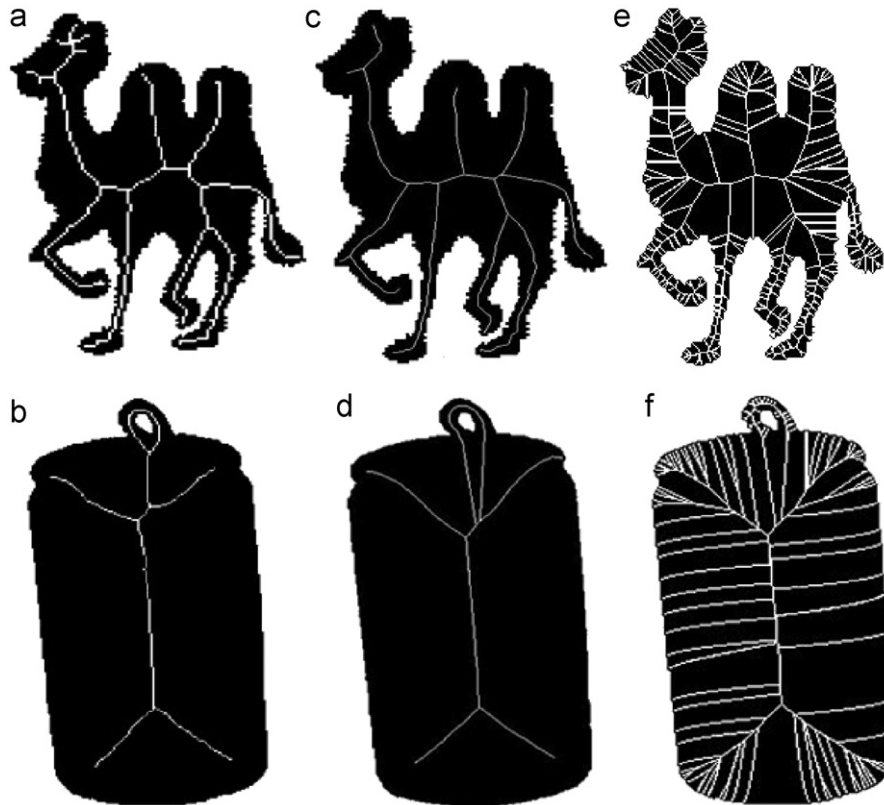


**Fig. 11.** Comparison between Krinidis's method [14] (a), (b) and ours (c), (d). The parameters in experiments are set as follows: (a)  $\alpha=300$ , (b)  $\alpha=300$ , (c)  $t=1.5$ , (d)  $t=0.3$ , (e) and (f) are the approximate Blum's skeletons.

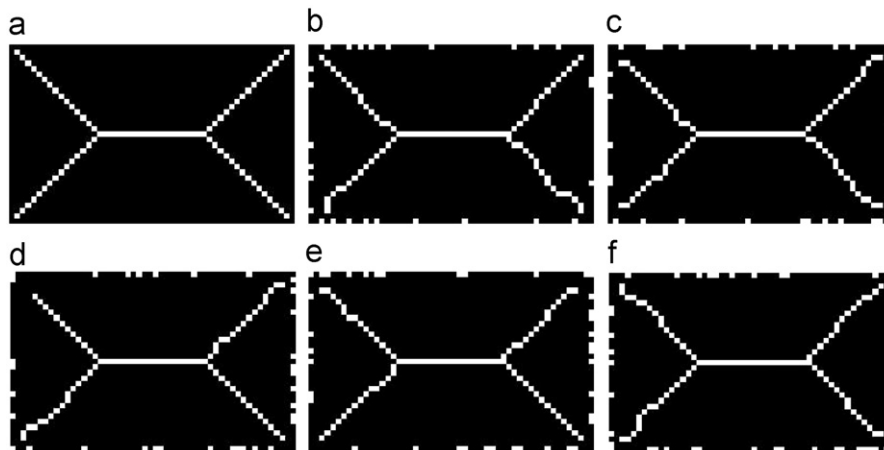


**Fig. 12.** Skeletons of six rectangles: (a) the original rectangle, (b) the rectangle with Gaussian noise (0, 1.0) on its boundary, (c) with Gaussian noise (0, 1.5), (d) with uniform noise (1.0), (e) with uniform noise (1.2), (f) with uniform noise (1.5). The threshold  $t$  is set equal to 0.8 in all experiments.

**Table 1**  
Skeletonization error in the examples presented in Fig. 12.

	Krinidis's method [14]	Pruned by DCE [20]	Pruned by the length of the shortest boundary segment [15]	Pruned by the length of chord [15]	Pruning by the bisector angle [17]	Our method
Average error pixel	0.31	0.28	0.27	0.39	0.44	0.25

In order to discuss the effect of the threshold  $t$  in-depth, we show the behavior of our method when the threshold is fixed. In [14], the result of extracting skeleton from several kinds of shapes with the threshold value  $\alpha=300$  is given. The result is quoted in

Fig. 18. We also give the result of skeletons of the same shapes as in [14] extracted by the proposed method using an equal threshold of  $t=1.0$  in Fig. 17. Our skeletons extracted with the same threshold are comparable to the skeletons given in [14].

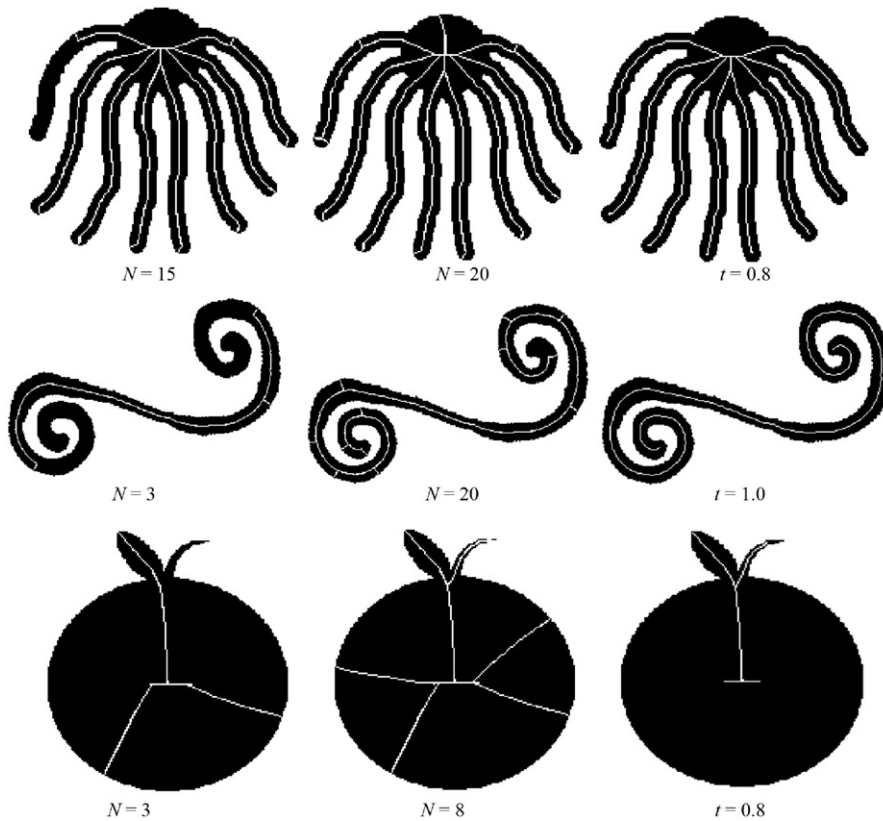


**Fig. 13.** Comparison between the method in [20] (the first two columns) and ours (the third column).  $N$  is the number of vertices selected by DCE,  $t$  is the threshold for significance measure BPR.

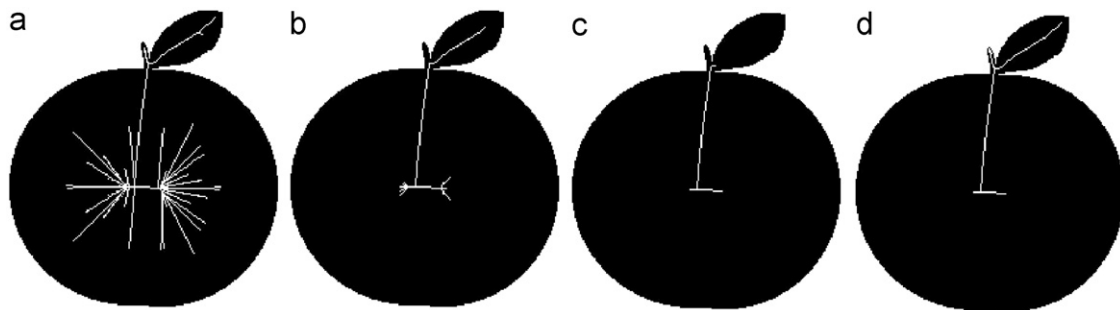


**Fig. 14.** Comparison between the significance measure of the length of the shortest boundary segment [15] (a), (b), (c) and ours (d). The threshold values of the length of the shortest boundary segment are 10, 30, 150 in (a), (b) and (c), respectively. The threshold value  $t=1.0$  in (d).

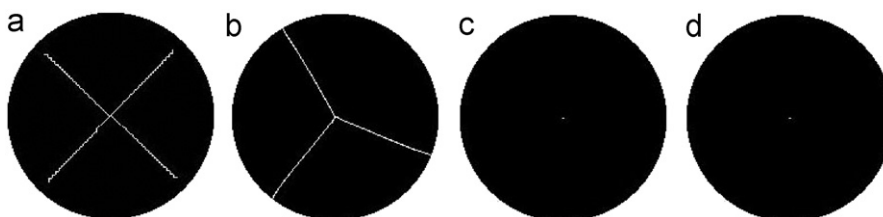


**Fig. 15.** Skeletons extracted from circles. (a) The skeleton obtained by the method in [34]. (b) The skeleton pruned by [20] with DCE set  $N=3$ . (c) (d) The skeletons extracted by our method with  $t=0.8$  and  $t=0.5$ , respectively.

To illustrate the accuracy of the skeletons obtained by different thresholds, we extract ten groups of skeletons from the rectangles in Fig. 12 by setting  $t$  of different values, and calculate the average

error pixel of each group by formula (14). The result is illustrated in Fig. 19, which indicates that the accuracy of our skeletons is stable when the variable quantity of  $t$  is within a certain range.

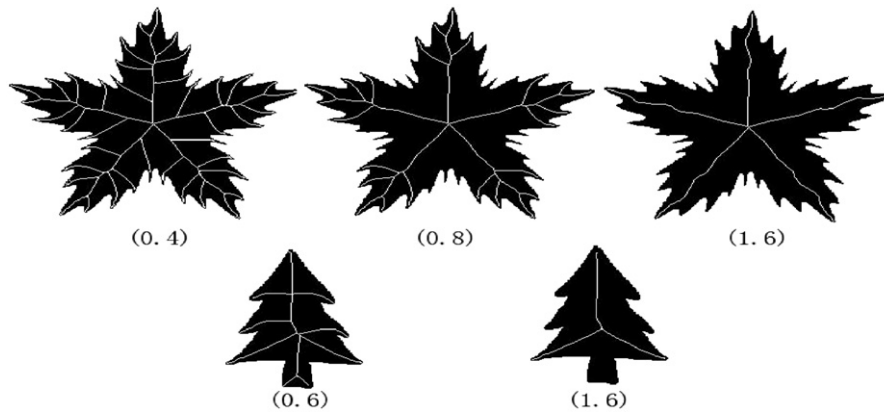


Fig. 16. First row: Multi-scale skeleton of a satellite shape. Second row: Multi-scale skeleton of a tree. The threshold values  $t$  set in experiment are shown in the brackets.

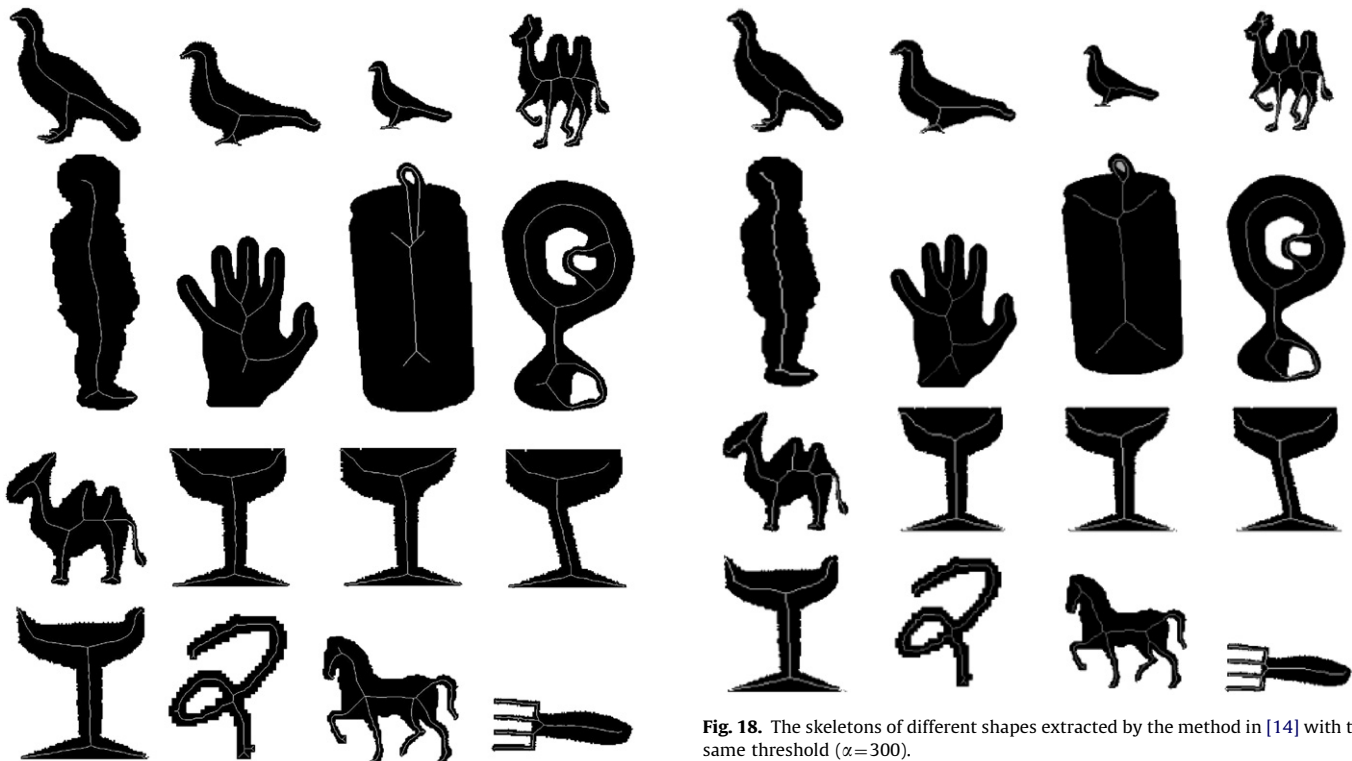


Fig. 17. The skeletons of different shapes extracted by the proposed method with the same threshold ( $t=1.0$ ).

Fig. 18. The skeletons of different shapes extracted by the method in [14] with the same threshold ( $\alpha=300$ ).

#### 5.4. Quantitative evaluation of skeleton quality

The skeleton of high quality should represent significant visual parts of objects. To evaluate this property of pruned skeletons, we compute a simple characteristic called reconstruction error ratio (RER), which can be used to measure the difference between the reconstructed shape and the original binary shape. Let  $S$  be a skeleton of shape  $A$  and let  $R(S)$  be the shape reconstructed from  $S$ , the RER  $\rho(S, A)$  is defined as

$$\rho(S, A) = \frac{\text{Area}(A) - \text{Area}(R(S))}{\text{Area}(A)}, \quad (15)$$

where  $\text{Area}(\cdot)$  denotes the area of a shape and it is measured in pixels. As demonstrated in Fig. 20a–e, the RER values are all very small; they are 0.0100, 0.0123, 0.0099, 0.0408, and 0.0097. This demonstrates the high quality of the obtained skeletons. We also show in Fig. 21 how the threshold  $t$  influences the RER.

#### 5.5. The potential for shape matching

The skeletons of the shapes from the same class always have similar global structures. Thus, shape matching can be achieved by establishing the optimal correspondence of the derived skeleton branches. The skeletons generated by the proposed method provide suitable input for shape matching due to their high quality as illustrated in Figs. 8 and 9. Since the skeletons provide a radius value for each skeleton point, they can be converted to shock graph [37–41] or bone graph [42] for matching. Here, we utilize the method proposed in [27] to measure the similarity of skeletons generated by the proposed method on the Aslan and Tari data set [47]. There are 14 classes of shapes in the Aslan and Tari data set; each class contains 4 shapes. Our retrieval result is 55, 55, and 53, which is the same as the result in [27] and better than the result obtained by inner distance shape context with dynamic programming [48], which is 53, 51, and 38. The retrieval results are summarized as the number of correct shapes for all 56 queries among the first, second, and third closest matches. Therefore, the

perfect result would be 56, 56, and 56. Some matching results are shown in Fig. 22; the corresponding skeleton branches are linked with green lines and marked with the same number.

Fig. 23 illustrates a comparison of shape matching to the method in [20]. In Fig. 23, the apple in the first row and the ellipse in the second row are two different shapes. Skeletons obtained by the proposed method and method in [20] are shown in Fig. 23a and b, respectively. The matching cost of the skeletons in Fig. 23b is 5.39, which is much less than ours, which is 16.82. This means it is easier to distinguish these two shapes by our skeletons. The matching costs are also computed by the method in [27].

### 6. Conclusions and future work

In this paper, we present a novel significance measure for skeleton pruning, called bending potential ratio. Based on this significance measure, we propose an algorithm for skeleton growing. Our experiments on MPEG-7 data set show that the obtained skeletons are medially placed, insensitive to boundary noise, multi-scale, and provide intuitive ordering of skeleton branches in that negligible skeleton branches are pruned while significant branches remain. The presented experimental results also demonstrate that our algorithm

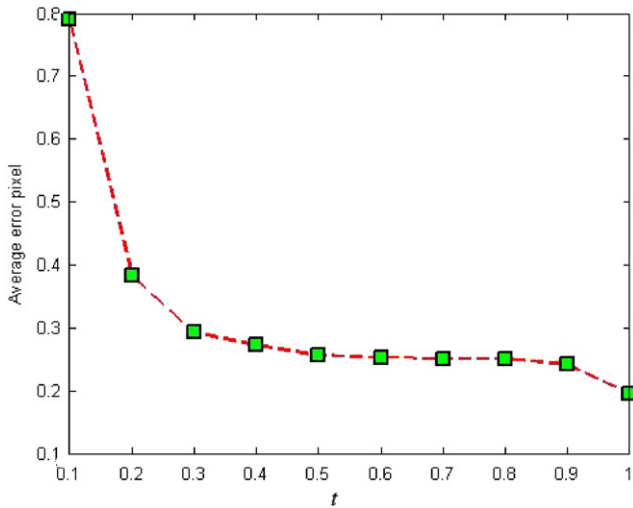


Fig. 19. The accuracy (average error pixel) of the skeletons obtained by using different thresholds.

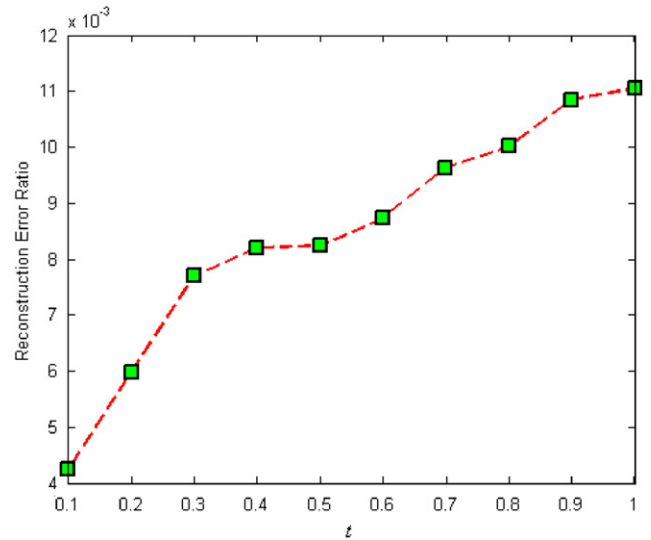


Fig. 21. The Reconstruction Error Ratio of skeletons of the shape in Fig. 20a for different values of threshold t.

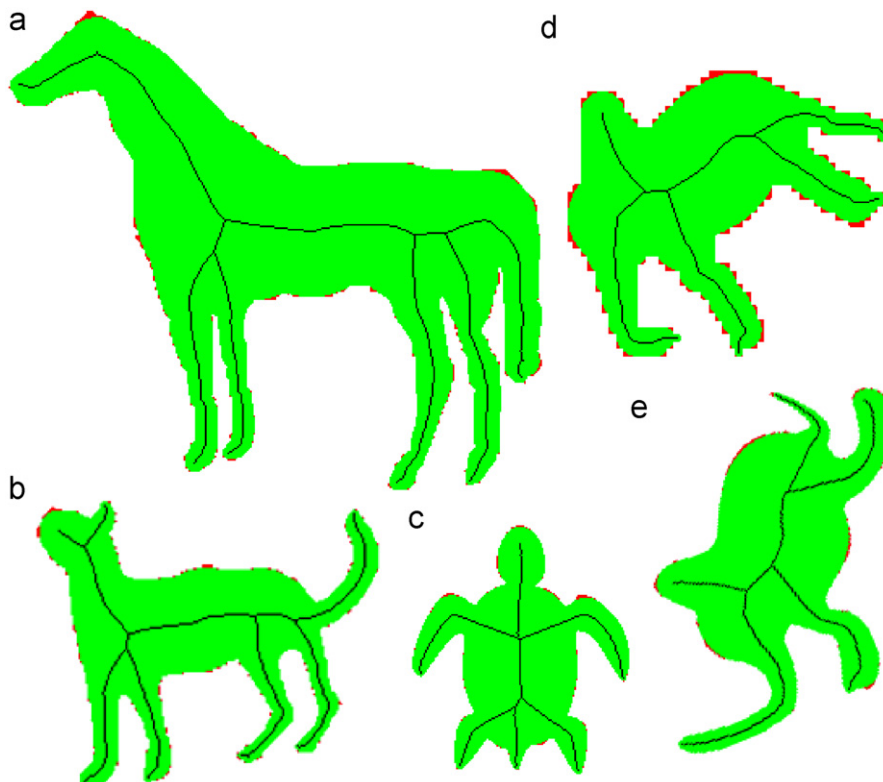


Fig. 20. Skeletons obtained by the proposed method. The shapes reconstructed from the skeletons are marked with green and the reconstruction errors are marked with red. The RER values of skeletons in (a)–(e) are 0.0100, 0.0123, 0.0099, 0.0408 and 0.0097, respectively.

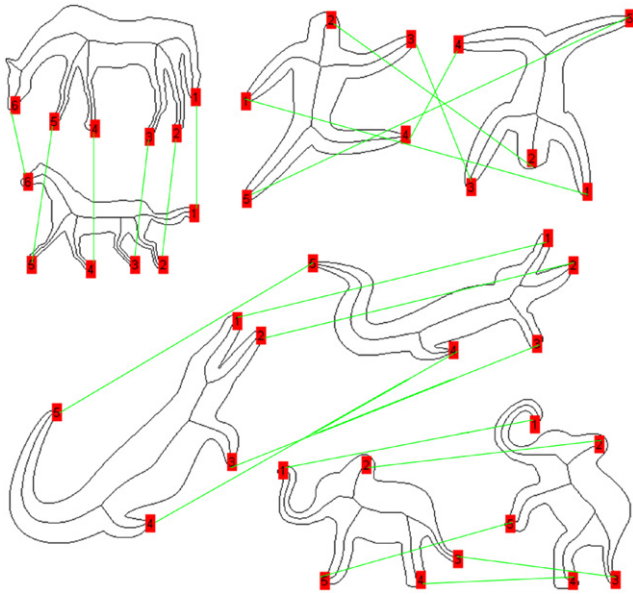


Fig. 22. Selected matching results on the Aslan and Tari data set. Corresponding skeleton branches are linked with green lines and marked with the same number.

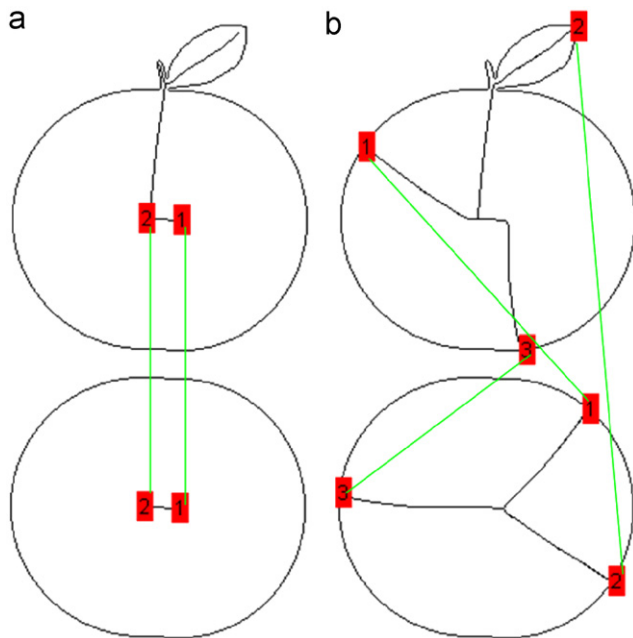


Fig. 23. Comparison between the method in [20]. (a) Skeletons obtained by proposed method, the matching cost is 16.82. (b) Skeletons obtained by the method in [20], the matching cost is 5.39. Corresponding skeleton branches are linked with green lines and marked with the same number.

generates skeletons of better quality than current state-of-the-art approaches. As an intrinsic property of contours, the proposed significance measure may be related to other properties, such as curvature. Besides, the ruling points associated with a skeleton point proposed in this paper are similar to the end points of the spokes associated with Blum's skeleton points. Our future work will include the relationship of the proposed bending potential to other geometric measures like local and global curvature.

## Acknowledgements

We would like to thank the three anonymous reviewers for their valuable comments that really improved the quality of this paper. This work was supported by the National Natural Science Foundation of China #60903096 and #60903172. This work is also in part supported by the Natural Science Foundation of Hebei Province F2009001435.

## References

- [1] H. Blum, in: *A Transformation for Extracting New Descriptors of Shape, Models for the Perception of Speech and Visual Form*, MIT Press, 1967 pp. 363–380.
- [2] H. Blum, *Biological shape and visual science (Part I)*, *J. Theoret. Biol.* 38 (1973) 205–287.
- [3] L. Lam, S.-W. Lee, C.Y. Suen, *Thinning methodologies—a comprehensive survey*, *IEEE Trans. Pattern Anal. Mach. Intell.* 14 (9) (1996) 869–885.
- [4] F. Leymarie, M. Levine, *Simulating the grassfire transaction form using an active contour model*, *IEEE Trans. Pattern Anal. Mach. Intell.* 14 (1) (1992) 56–75.
- [5] R. Ogniewicz, M. Ilg, *Voronoi skeletons: theory and applications*, in: *Proceedings of the Conference on Computer Vision and Pattern Recognition*, 1992, pp. 63–69.
- [6] J.W. Brandt, V.R. Algazi, *Continuous skeleton computation by Voronoi diagram*, *CVGIP: Image Understanding* 55 (3) (1992) 329–338.
- [7] C.W. Niblack, P.B. Gibbons, D.W. Capson, *Generating skeletons and centerlines from the distance transform*, *CVGIP: Graphical Models Image Process.* 54 (5) (1992) 420–437.
- [8] N. Mayya, V.T. Rajan, *Voronoi diagrams of polygons: a framework for shape representation*, in: *Proceedings of the Conference on Computer Vision and Pattern Recognition*, 1994, pp. 638–643.
- [9] P. Dimitrov, J.N. Damon, K. Siddiqi, *Flux invariants for shape*, in: *Proceedings of the Conference on Computer Vision and Pattern Recognition*, 2003, pp. 835–841.
- [10] P. Golland, W.E.L. Grimson, *Fixed topology skeletons*, in: *Proceedings of the Conference on Computer Vision and Pattern Recognition*, 2000, pp. 10–17.
- [11] Y. Ge, J.M. Fitzpatrick, *On the generation of skeletons from discrete euclidean distance maps*, *IEEE Trans. Pattern Anal. Mach. Intell.* 18 (11) (1996) 1055–1066.
- [12] W.-P. Choi, K.-M. Lam, W.-C. Siu, *Extraction of the euclidean skeleton based on a connectivity criterion*, *Pattern Recognition* 36 (2003) 721–729.
- [13] D. Shaked, A.M. Bruckstein, *Pruning medial axes*, *Comput. Vision Image Understanding* 69 (2) (1998) 156–169.
- [14] S. Krinidis, V. Chatzis, *A skeleton family generator via physics-based deformable models*, *IEEE Trans. Image Process.* 18 (1) (2009) 1–11.
- [15] R.L. Ogniewicz, O. Kübler, *Hierarchical Voronoi skeletons*, *Pattern Recognition* 28 (3) (1995) 343–359.
- [16] L. Gorelick, M. Galun, E. Sharon, R. Basri, A. Brandt, *Shape representation and classification using the poisson equation*, *IEEE Trans. Pattern Anal. Mach. Intell.* 28 (12) (2006) 1991–2005.
- [17] M. Couprie, R. Zrou, *Discrete bisector function and euclidean skeleton in 2D and 3D*, *Image Vision Comput.* 25 (10) (2007) 1543–1556.
- [18] A.D. Ward, G. Hamarneh, *The groupwise medial axis transform for fuzzy skeletonization and pruning*, *IEEE Trans. Pattern Anal. Mach. Intell.* 32 (6) (2010) 1084–1096.
- [19] X. Bai, X.-W. Yang, L.J. Latecki, W.-Y. Liu, and Z.-W. Tu, *Learning context sensitive shape similarity by graph transduction*, *IEEE Trans. Pattern Anal. Mach. Intell.* 32 (5) (2010) 861–874.
- [20] X. Bai, L.J. Latecki, W.-Y. Liu, *Skeleton pruning by contour partitioning with discrete curve evolution*, *IEEE Trans. Pattern Anal. Mach. Intell.* 29 (3) (2007) 449–462.
- [21] L.J. Latecki, R. Lakämper, *Convexity rule for shape decomposition based on discrete contour evolution*, *Computer Vision Image Understanding* 73 (1999) 441–454.
- [22] Z.-Y. Yu, C. Bajaj, *A segmentation-free approach for skeletonization of gray-scale images via anisotropic vector diffusion*, *CVPR* (2004) 415–420.
- [23] C. Aslan, A. Erdem, E. Erdem, S. Tari, *Disconnected skeleton: shape at its absolute scale*, *IEEE Trans. Pattern Anal. Mach. Intell.* 30 (12) (2008) 2188–2203.
- [24] M. Leyton, *A process-grammar for shape*, *Artif. Intell.* 34 (2) (1988) 213–247.
- [26] L.J. Latecki, R. Lakamper, U. Eckhardt, *Shape descriptors for non-rigid shapes with a single closed contour*, in: *Proceedings of the Conference on Computer Vision and Pattern Recognition*, 2000, pp. 424–429.
- [27] X. Bai, L.J. Latecki, *Path similarity skeleton graph matching*, *IEEE Trans. Pattern Anal. Mach. Intell.* 30 (7) (2008) 1282–1292.
- [28] C.-J. Xu, J.-Z. Liu, X.-O. Tang, *2D shape matching by contour flexibility*, *IEEE Trans. Pattern Anal. Mach. Intell.* 31 (1) (2009) 180–186.
- [29] C. Arcelli, G. Sanniti di Baja, *A width-independent fast thinning algorithm*, *IEEE Trans. Pattern Anal. Mach. Intell.* 7 (4) (1985) 463–474.

- [30] C. Arcelli, G. Sanniti di Baja, A one-pass two-operations process to detect the skeletal pixels on the 4-distance transform, *IEEE Trans. Pattern Anal. Mach. Intell.* 11 (4) (1989) 411–414.
- [31] G. Sanniti di Baja, Well-shaped, stable and reversible skeletons from the (3,4)-distance transform, *J. Visual Comm. Image Representat.* 5 (1994) 107–115.
- [32] G. Sanniti di Baja, E. Thiel, Skeletonization algorithm running on path-based distance maps, *Image Vision Comput.* 14 (1) (1996) 47–57.
- [33] C. Arcelli, G. Sanniti di Baja, Euclidean skeleton via center-of-maximal-disc extraction, *Image Vision Comput.* 11 (3) (1993) 163–173.
- [34] Alexandru Telea and Jarke J. van Wijk, An augmented fast marching method for computing skeletons and centerlines. In: *IEEE TCVG Symposium on Visualization*, 2002, pp. 251–259.
- [35] X. Bai, L.J. Latecki, Discrete skeleton evolution, *EMMCVPR (2007)* 274–362.
- [36] P. Dimitrov, C. Phillips, and K. Siddiqi, Robust and efficient skeletal graphs, in: *Proceedings of the Conference on Computer Vision and Pattern Recognition*, 2000, pp. 1417–1423.
- [37] K. Siddiqi, A. Shokoufandeh, S.J. Dickinson, S.W. Zucker, Shock graphs and shape matching, *Int. J. Comput. Vision* 35 (1) (1999) 13–32.
- [38] M. Pelillo, K. Siddiqi, S. Zucker, Matching hierarchical structures using association graphs, *IEEE Trans. Pattern Anal. Mach. Intell.* 21 (11) (1999) 1105–1120.
- [39] K. Siddiqi, S. Bouix, A.R. Tannenbaum, S.W. Zucker, Hamilton–Jacobi skeletons, *Int. J. Comput. Vision* 48 (3) (2002) 215–231.
- [40] K. Siddiqi, B.B. Kimia, A shock grammar for recognition, *CVPR (1996)* 507–513.
- [41] T. Sebastian, P. Klein, B.B. Kimia, Recognition of shapes by editing their shock graphs, *IEEE Trans. Pattern Anal. Mach. Intell.* 26 (5) (2004) 550–571.
- [42] D. Macrini, K. Siddiqi, S. Dickinson, From skeletons to bone graphs: medial abstraction for object recognition, *CVPR (2008)*.
- [43] X. Bai, X. Yang, D. Yu, L.J. Latecki, Skeleton-based shape classification using path similarity, *Int. J. Pattern Recog. Artif. Intell.* 22 (4) (2008) 733–746.
- [44] X. Bai, W. Liu, and Z. Tu, Integrating contour and skeleton for shape classification, *IEEE Workshop on NORDIA*, 2009.
- [45] X. Bai, X. Wang, L.J. Latecki, W. Liu, Z. Tu, Active skeleton for non-rigid object detection, *ICCV (2009)*.
- [46] K. Siddiqi, B.B. Kimia, C. Shu, Geometric shock-capturing ENO schemes for subpixel interpolation, computation, and curve evolution, *ISCV (1995)*.
- [47] C. Aslan, S. Tari, An axis based representation for recognition, in: *Proceedings of the Conference on Computer Vision*, 2005, pp. 1339–1346.
- [48] H. Ling, D.W. Jacobs, Shape classification using inner-distance, *IEEE Trans. Pattern Anal. Mach. Intell.* 29 (2) (2007) 286–299.

**Wei Shen** received his B.S. degree in Electronics and Information Engineering from the Huazhong University of Science and Technology (HUST), Wuhan, China, in 2007. Currently, he is a Ph.D. candidate at HUST.

**Xiang Bai** received his B.S. and M.S. degree both in electronics and information engineering from Huazhong University of Science and Technology (HUST), Wuhan, China, in 2003 and in 2005, respectively. He obtained his Ph.D. degree from HUST in 2010. From January 2006 to May 2007, he worked in the Department of Computer Science and Information, Temple University. From October 2007 to October 2008, he worked in the University of California, Los Angeles as a joint Ph.D. student. Now he is a faculty of EI Department, HUST. His research interests include computer graphics, computer vision, and pattern recognition.

**Rong Hu** received his B.S. degree in Electronics and Information Engineering from the Huazhong University of Science and Technology (HUST), Wuhan, China, in 2005. Now, he is a Ph.D. candidate at HUST.

**Hongyuan Wang** is a professor of the Department of Electronics and Information Engineering at the Huazhong University of Science and Technology. From 1984 to 1985, he worked in the University of Oklahoma as a visiting scholar. His current research areas include digital video communication and digital signal processing.

**Longin Jan Latecki** is an associate professor in the Department of Computer and Information Sciences at the Temple University in Philadelphia. He is the winner of the 25th Pattern Recognition Society Award together with Azriel Rosenfeld for the best paper published in the journal *Pattern Recognition* in 1998. He received the main annual award from the German Society for Pattern Recognition (DAGM), the 2000 Olympus Prize. He is a member of the Editor Board of *Pattern Recognition* and chairs the IS&T/SPIE annual conference series on Vision Geometry. He has published and edited over 150 research articles and books. His main research areas are shape representation and shape similarity, object recognition, robot mapping, video analysis, data mining, and digital geometry.